JOURNAL OF SOLID STATE CHEMISTRY 110, 74–79 (1994)

New Defective Brannerite-Type Vanadates

I. Synthesis and Study of $Mn_{1-x-y}\phi_xNa_yV_{2-2x-y}Mo_{2x+y}O_6$ Solid Solutions

Bogna Masłowska and Jacek Ziółkowski[1]

Institute of Catalysis and Surface Chemistry, Polish Academy of Sciences, 30-239 Kraków, ul. Niezapominajek, Poland

Received April 12, 1993; in revised form August 3, 1993; accepted August 5, 1993

MnV_2O_6 of the brannerite-type structure (below 540°C) doped with MoO_3 and Na_2O forms isomorphous solid solutions $MnNa\phi = Mn_{1-x-y}\phi_xNa_yV_{2-2x-y}Mo_{2x+y}O_6$ (ϕ, cation vacancy in the original Mn position), belonging to the pseudoternary MnV_2O_6–$NaVMoO_6$–MoO_3 system. Particular cases are $MnNa = Mn_{1-y}Na_yV_{2-y}Mo_yO_6$ ($x = 0$), $Mn\phi = Mn_{1-x}\phi_xV_{2-2x}Mo_{2x}O_6$ ($y = 0$), and $Na\phi = Na_{1-x}\phi_xV_{1-x}Mo_{1+x}O_6$ ($x + y = 1$). MnV_2O_6 and $NaVMoO_6$ show miscibility in the entire composition range (MnNa). The opposite boundary of $MnNa\phi$ passes through the ($100x$, $100y$) points (45, 0), (33, 30), and (30, 70). The phase diagram of the pseudobinary MnV_2O_6–$NaVMoO_6$ system (determined with DTA) shows (i) a narrow double-lens-type solidus–liquidus gap at high values of y, (ii) two peritectic meltings at lower y (yielding the high temperature β-MnNa and $Mn_2V_2O_7$), and (iii) little area of β-MnNa. Lattice parameters of MnNa (determined with X-ray diffraction) reveal small deviations from Vegard's law. As the ionic radii of both dopants (Na^+ and Mo^{6+}) are, respectively, larger than those of mother ions (Mn^{2+} and V^{5+}), the unit cell increases in all directions with rising y along the MnNa series of solid solutions. However, due to the anisotropy of the structure, parameter c is strongly sensitive to Na/Mn substitution, b is ruled by Mo/V, and a is weakly influenced by Mo/V. Close analogy to the behavior of the previously studied MnV_2O_6–$LiVMoO_6$–MoO_6 system is discussed.

1. INTRODUCTION

Since 1980, systematic investigations have been carried out in our laboratory on the defective brannerite-type vanadates. In this work, we intend to report some new results in this field.

A number of bivalent metal vanadates MeV_2O_6 (Me = Mg, Mn, Co, Cu, Zn, Cd) crystallize in the monoclinic brannerite-type structure or are exhibited by at least one of the polymorphs (1). In this structure (2), visualized in Fig. 1, distorted VO_6 octahedra sharing edges and corners form the anionic sheets parallel to (001), with packing tight along [010] and less tight along [100]. Edge sharing, distorted MeO_6 octahedra make isolated [010] pillars linking the anionic layers in the [001] direction. The same structure is adapted by $LVMoO_6$ (L = Li, Na, Ag) compounds (3, 4).

We have shown (Ref. (5) and papers quoted therein) that random isomorphous substitutions of Mo^{6+} for V^{5+} and Li^+ for Me^{2+} are possible in the MeV_2O_6 matrices and $MeLi\phi$ solid solutions are formed: $MeLi\phi = Me_{1-x-y}\phi_xLi_yV_{2-2x-y}Mo_{2x+y}O_6$, ϕ = cation vacancy in the original Me sublattice. The stability ranges of these solutions are very large; y can usually vary from 0 to 1 (or close to 0 for Me = Co (1)) and x_{max} even reaches 0.45 (if Me = Mn (6)).

The stoichiometry of $MeLi\phi$ may be expressed as $Me_{1-x-y}\phi_xLi_yV_{2-2x-y}Mo_{2x+y}O_6 = (1 - x - y)\,MeV_2O_6 + y\,LiVMoO_6 + 2x\,MoO_3$. $MeLi\phi$ solutions thus belong to the pseudoternary MeV_2O_6–$LiVMoO_6$–MoO_3 system and their composition may be represented using the equilateral triangle (cf. Fig. 2, little triangle) with composition variables $X = 100x$ and $Y = 100y$ marked along the MeV_2O_6–MoO_3 and MeV_2O_6–$LiVMoO_6$ arms, respectively.

At $Y = 0$, $X = 0$, and $X + Y = 100$ we deal, respectively, with the pseudobinary solid solutions $Me\phi = Me_{1-x}\phi_xV_{2-2x}Mo_{2x}O_6$ (MeV_2O_6–MoO_3 arm of the triangle), $MeLi = Me_{1-y}Li_yV_{2-y}Mo_yO_6$ (MeV_2O_6–$LiVMoO_6$ arm), and $Li\phi = Li_{1-x}\phi_xV_{1-x}Mo_{1+x}O_6$ ($LiVMoO_6$–MoO_3 arm).

Taking into account that $NaVMoO_6$ makes the analogous $Na\phi$ solid solutions in a wide range ($0 \le X \le 30$) (4), we can expect the existence of $MeNa$ and $MeNa\phi$. In the present paper we intend to offer the proofs of the validity of this hypothesis for Me = Mn.

In view of the changeable chemical composition of the discussed phases, it will be convenient sometimes to use the general formula of brannerites AB_2O_6 and to speak about AO_6 and BO_6 octahedra, with the understanding that A = Li/Na/Mn/ϕ and B = V/Mo in different proportions.

[1] To whom correspondence should be addressed.

0022-4596/94 $6.00

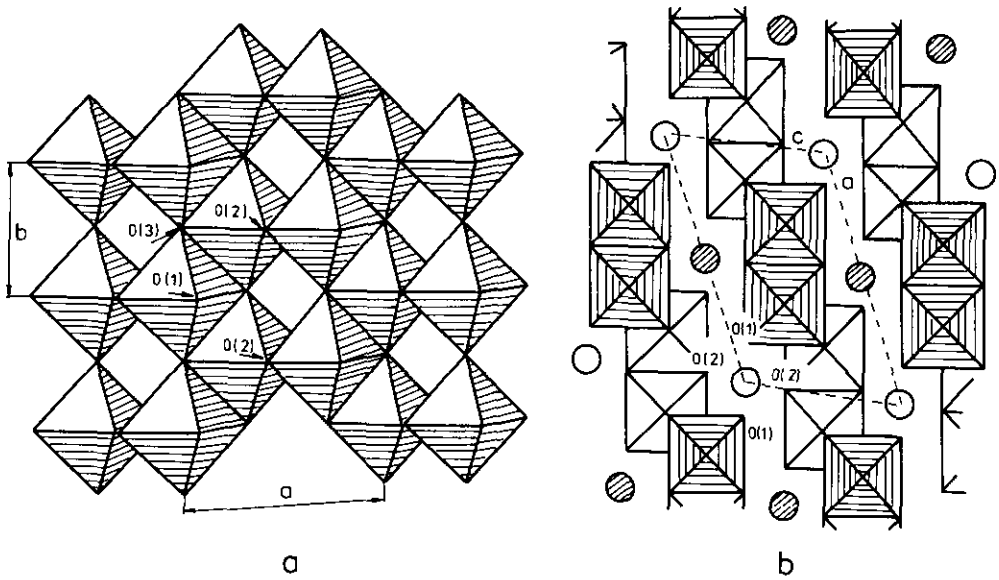

FIG. 1. Idealized outline of the brannerite-type MeV_2O_6 structure (after (2)). (a) A sheet of VO_6 octahedra parallel to the (001) plane (nonequivalent oxygens linked with one, two, or three vanadium atoms are labeled O(1), O(2), and O(3), respectively). (b) Projection of the structure on the (010) plane with marked *Me* cations and VO_6 groups on two different levels (0 and 0.5 of *b*).

2. EXPERIMENTAL

The composition of all samples prepared and studied with X-ray analysis and partly with DTA is marked in Fig. 2. Samples were synthesized by the amorphous citrate precursor method (7), adapted empirically to the present systems (6). Reactants were Na_2CO_3, $MnCO_3$, NH_4VO_3 $(NH_4)_6Mo_7O_{24} \cdot 4H_2O$, 0.1 *M* HNO_3, 2.5 *M* citric acid, and 0.1 *M* ammonia, all of p.a. grade. The procedure has been described in (6); the final thermal treatment was carried out in air at 530°C for 24 hr; thereafter, the samples were quenched.

X-ray diffraction patterns were obtained with DRON-2 diffractometer using Cu$K\alpha$ radiation and an internal standard of Al (a = 4.0492 Å at 25°C). Data were collected on a floppy disc and processed with the SMOK (Elector Co., Kraków, Poland) and LATCON (CERN library) programs. Reflections of $25 < 2\theta < 60°$ were used to determine the lattice constants. Phase identification was based on the published patterns of MnV_2O_6 (8), $NaVMoO_6$ (3), MoO_3 (9), and $MnMoO_4$ (10). Elemental analysis (Pye-Unicam FP 90 spectrometer), DTA (Setaram M5 microanalyzer, 10°/min, Pt crucibles, samples of 12.5 mg), and treatment of DTA curves were performed as described previously (5, 6).

3. RESULTS AND DISCUSSION

3.1. Range of Stability of MnNaϕ

Mnϕ solid solutions have been described in (8); their stability range is $0 \leq X \leq 45$. The range of Naϕ, determined in (4) and confirmed in our laboratory, is $0 \leq X \leq 30$. The composition of the studied MnNa and MnNaϕ samples is indicated in Fig. 2 (solid and open circles). We proved gravimetrically that during the thermal treatment there is no loss of material exceeding that expected due to volatiles or combustion products. Elemental analyses of the chosen samples, performed after the final thermal treatment, also confirmed the intended stoichiometry. X-ray phase analysis revealed that all samples of the compositions marked in Fig. 2 with solid circles give the diffraction pattern of pure brannerite, entirely indexable in a monoclinic system with systematic extinctions for $h + k = 2n + 1$. The stability range of MnNaϕ comprises nearly 60% of the triangle area and extends between the MnV_2O_6–$NaVMoO_6$ arm and the S_1S_2 curve, slightly concave with respect to this arm. The S_1S_2 curve can be approximated by two straight segments between the (X, Y)-points: (45, 0), (30, 30), and (30, 70). Behind the S_1S_2 boundary we deal with a multiphasic area (samples of the composition marked in Fig. 2 with open circles). A number of nonbrannerite X-ray reflections appear with intensities that increase as indicated by arrows. The presence of $MnMoO_4$ and strongly oriented MoO_3 (with predominant (040) reflection) has been identified unequivocally. Some unassigned reflections (8.61, 5.83, 5.60, 5.10 Å) prove that at least one additional phase is present. The obtained stability diagram of MnNaϕ (Fig. 2) strongly resembles that for MnLiϕ (6), briefly recalled in the upper part of Fig. 2. The following features are common to both diagrams: (i) complete miscibility of MnV_2O_6 and $LVMoO_6$, (ii) large stability area of MnLϕ, and (iii) nearly linear (slightly

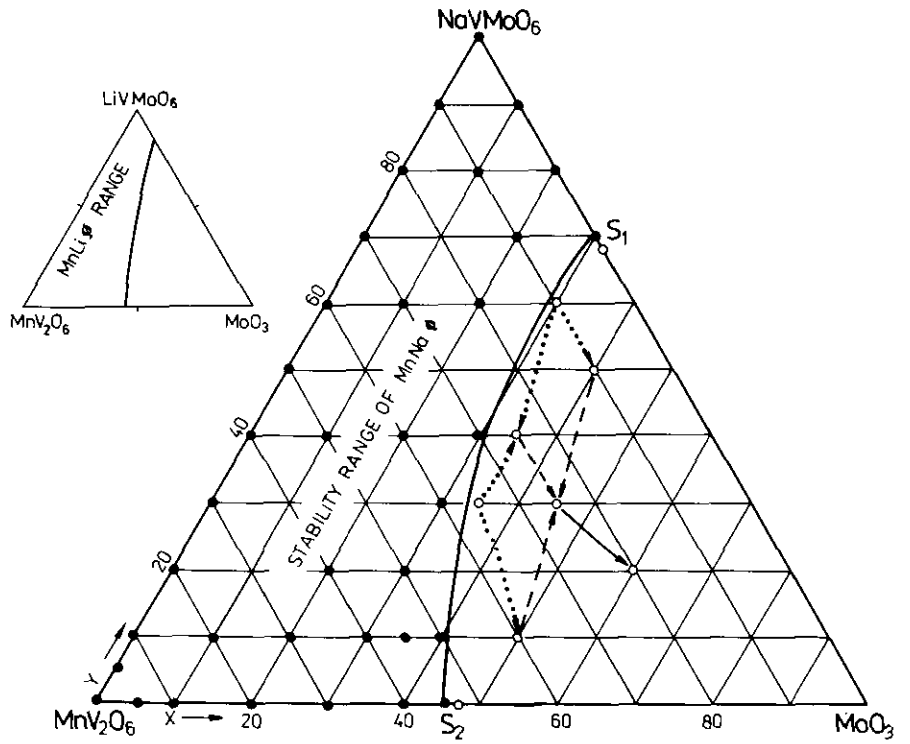

FIG. 2. The area of stability of the MnNaϕ solid solutions. Solid circles correspond to the studied samples composed of single brannerite-type phase. Open circles, behind the S_1S_2 boundary, represent studied samples contaminated with MoO_3, $MnMoO_4$, and at least one unidentified phase. Arrows indicate the increasing degree of contamination, stressed by using the dotted, dashed, and full lines. The stability range of MnLiϕ (6) is recalled in the upper part of the figure.

concave) boundary of the saturated MnLϕ solutions. The differences consist in (i) smaller range of stability of Liϕ ($0 \leq x \leq 16$) as compared to Naϕ ($0 \leq X \leq 30$), and (ii) monophasic (MoO_3) area behind the boundary of saturated MnLiϕ, and a multiphasic area outside the saturated MnNaϕ ($MnMoO_4$ + MoO_3 + at least one nonidentified phase).

3.2. *Lattice Parameters of MnNa*

The determined lattice constants of MnNa solid solutions are listed in Table 1 along with their relative changes $\Delta p\%$ between the end members of the series (p = parameter a, b . . . , $\Delta p\% = 100\ \Delta p/p_{Y=0}$). The revised data for $LiVMoO_6$ and $\Delta p\%$ values for the MnLi series of solid solutions (6) are also included for comparison. The parameter-composition plots for MnNa and MnLi are shown in Fig. 3.

As already discussed in Ref. (5), there are three factors which should influence the lattice constants of this structure: (i) the sequence of packing of the two kinds of AO_6 and BO_6 octahedra, (ii) the anisotropic tightness of the packing (related to the space-differentiation of the bond lengths), and (iii) the size of ions.

—The sequence of packing has already been discussed in the Introduction: AO_6 octahedra share edges in the [010] direction and have no links in [100]; BO_6 octahedra make a planar (001) "lattice"; $(AO_6)_n$ pillars and $(BO_6)_{2n}$ sheets alternate along [001].

—The tightness of packing may be derived from the lengths of edges and diagonals of octahedra in the structure. In all brannerite-type vanadates for which the structures have been resolved, the proportions between the bond lengths in AO_6 and BO_6 octahedra are nearly the same. Therefore, we make use of the data for $NaVMoO_6$ (4) gathered in Table 2. It is clear from the table that AO_6 octahedra are tight in [100] and [001] but bulky in [010]; BO_6 are tight in [010] and bulky in [100] and [001].

—A set of the relevant ionic radii is gathered in Table 3 along with their relative changes $\Delta r\%$ between the end members of the considered MnNa and MnLi solid solutions. $\Delta r\%$ values are defined as, e.g.,

$$\Delta r\%(\mathrm{Na/Mn}) = 100\frac{r_{Na^{1+}} - r_{Mn^{2+}}}{r_{Mn^{2+}}}. \qquad [1]$$

An increase of Y along the MnNa or MnLi series of solutions is equivalent to the rising extent of substitution of Mo for V (from 0 to 1/2) and Na or Li for Mn (from 0 to 1). As the cations are "diluted" in the structure with oxygens of constant size, the $\Delta r\%$ values can be used to identify the trends in changes of lattice parameters along the series of solutions. It is significant that in the MnNa

TABLE 1
Lattice Parameters for the MnNa = $Mn_{1-y}Li_yV_{2-y}Mo_yO_6$ Solid Solutions and the Relative Changes $\Delta p\%$ between the End Members of the Series

Y	a (Å)	b (Å)	c (Å)	β (deg)	$c \sin \beta$ (deg)	V (Å^3)
			MnNa series			
0	9.315(3)	3.536(1)	6.754(2)	112.66(2)	6.233(2)	205.29(20)
10	9.334(3)	3.550(1)	6.790(2)	112.60(2)	6.628(2)	207.69(20)
20	9.345(3)	3.564(1)	6.834(3)	112.59(2)	6.312(4)	210.24(20)
30	9.367(5)	3.574(1)	6.873(4)	112.53(2)	6.384(5)	212.53(33)
40	9.380(2)	3.589(1)	6.928(2)	112.51(1)	6.400(2)	215.46(17)
50	9.396(3)	3.600(1)	6.969(3)	112.57(1)	6.449(3)	218.15(22)
60	9.407(3)	3.612(1)	7.022(2)	112.22(1)	6.501(2)	220.88(21)
70	9.412(2)	3.624(1)	7.076(3)	111.93(1)	6.564(3)	223.89(21)
80	9.417(3)	3.632(1)	7.119(2)	111.83(1)	6.609(2)	226.03(22)
90	9.426(4)	3.646(1)	7.197(5)	111.32(4)	6.704(7)	230.41(39)
100	9.430(4)	3.656(1)	7.257(4)	111.01(2)	6.775(4)	233.56(32)
$\Delta p\%$MnNa	1.24	3.36	7.37		8.38	13.48
			$LiVMoO_6$			
	9.346(2)	3.650(1)	6.637(1)	111.65(1)	6.168(1)	210.43(14)
			MnLi series			
$\Delta p\%$MnLi	0.33	3.22	−1.73		−1.04	2.50

Note. Standard deviation is given in parentheses. The revised parameters for $LiVMoO_6$ and $\Delta p\%$ for MnLi are included for comparison.

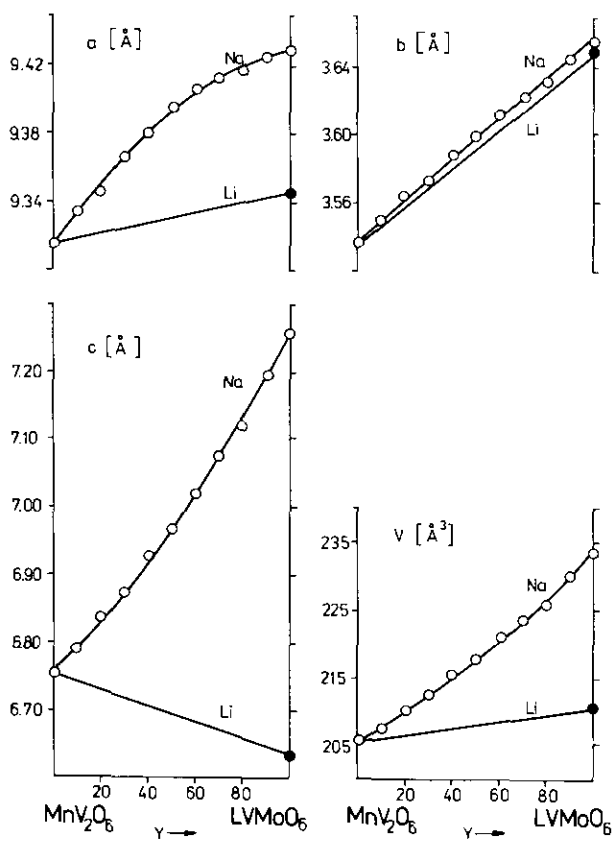

FIG. 3. Lattice parameters of MnNa solid solutions as a function of composition (cf. Table 1). For comparison, the data for MnLi are included.

series both $\Delta r\%$(Mo/V) and $\Delta r\%$(Na/Mn) are positive; therefore, the increase of all parameters (a, b, c, V) is expected which is indeed experimentally observed. On the contrary, in the MnLi series $\Delta r\%$(Mo/V) is positive while $\Delta r\%$(Li/Mn) is negative; the competition of the opposite effects results in an increase of a, b, and V and a decrease of c along the MnLi series.

Let us now compare the size of ions and the manner and tightness of their packing with the anisotropic $\Delta p\%$ values. $\Delta a\%$ is positive and the smallest in both series of solid solutions. This is due to the fact that BO_6 octahedra are bulky in [100] and offer enough space for Mo^{6+} to be substituted for V^{5+}; on the other hand, the AO_6 octahedra have no links in this direction; thus, the a-parameter is not especially sensitive to the size of A. Therefore, $\Delta a\%$ is ruled mainly by $\Delta r\%$(Mo/V), the effect being small due to the loose packing in [100].

It is striking that $\Delta b\%$ is almost the same for MnNa and MnLi. This means that b is sensitive solely to Mo/V substitutions. Indeed, BO_6 are tight in [010] while AO_6 are very bulky in this direction.

$\Delta c\%$ is positive for MnNa and negative for MnLi. As BO_6 are bulky in [001], we can expect that the thickness of $(BO_6)_{2n}$ sheets is almost constant along both series of solutions. On the other hand, AO_6 are tight in [001]. $\Delta c\%$ is thus ruled by $\Delta r\%$(Na/Mn) and $\Delta r\%$(Li/Mn). The first of them is positive; consequently, c increases along MnNa. The second is negative; thus, c decreases along MnLi. It seems worth mentioning that the ratio

TABLE 2
The Lengths (in Å) of Edges (E) and Diagonals (D) of Octahedra in $NaVMoO_6$

Octahedron	E	D	Direction traced by E/D is close to
AO_6	3.25		[100]/[101]
	3.66		[010]
		4.58	[001]
		4.88 twice	[010]
BO_6	2.71 aver. of 4		[010]
	2.77 aver. of 2		[100]/[101]
	2.81 aver. of 2		[001]
		3.66	[010]
		3.77	[10$\bar{1}$]
		4.10	[101]

$\Delta c\%(Mn/Na)/|\Delta c\%(Li/Mn)|$ is about 4, while the respective ratio of $\Delta r\%$ values is about 3, the numbers being comparable.

Finally, we would like to note that the parameter–composition plots for MnLi strictly follow Vegard's rule and slight deviation from linearity is observed for the MnNa plots. This character of MnLi and MnNa remains in opposition to the properties of MgLi, CoLi, and ZnLi (5), in which significant deviations from Vegard's law were observed, especially for the c-parameter.

3.3. *Phase Diagram of the MnV_2O_6-$NaVMoO_6$ System*

Based on DTA, the phase diagram of the pseudobinary MnV_2O_6–$NaVMoO_6$ system has been determined as shown in Fig. 4a. The onset temperatures of endothermal effects (solid circles) and their endings (open circles) have been determined accurately (±2°C). Positions of other effects, manifesting as shoulders or poorly separated peaks, were estimated tentatively (crosses). The identification of areas is based on the coincidence of the present diagram and that of the MoO_3–MnV_2O_6 system, studied previously (6) and recalled on the left of Fig. 4a. The characteristic points of the diagram will be indicated by their (Y, temperature) coordinates.

MnV_2O_6 is known (6, 8) to undergo a reversible phase transformation at (0, 540). The low temperature α-modification crystallizes in the brannerite-type, while the structure of the high temperature β-polymorph is not known (see Ref. (8) for the nonindexed powder X-ray pattern). At (0, 825), β-MnV_2O_6 melts incongruently, decomposing to $Mn_2V_2O_7$ and liquid. The liquidus line in the MnO–V_2O_5 system over MnV_2O_6 is attained at (0, 935).

On increasing Y ("doping" with $NaVMoO_6$), MnNa solid solutions are formed in both α and β modifications of MnV_2O_6. The extent of solid solubility in β is very small and attains its largest value (8, 648). There is a narrow "triangular" field of α-MnNa + β-MnNa coexistence between (0, 540), (8, 648), and (25, 648), its existence being a simple consequence of the phase rule. An attempt was made to confirm this area by high-temperature X-ray diffraction. It appeared, however, that the $\alpha \rightarrow \beta$ transition is accompanied by strains that deform the sample in the high temperature sample holder and preclude completing the experiment.

α-MnV_2O_6 and $NaVMoO_6$ show miscibility in the entire composition range. Incorporation of dopants stabilizes α-MnNa against the $\alpha \rightarrow \beta$ transformation. At (25, 648), α-MnNa, revealing the highest thermal stability among the α-type solutions, melts incongruently, decomposing to β-MnNa and liquid, represented by (8, 648) and (62, 648), respectively. Upon heating the samples of $8 < Y < 37$ above 648°C, and before the total melting, one crosses the areas of coexistence of $Mn_2V_2O_7$ + β-MnNA + liquid and $Mn_2V_2O_7$ + liquid. On heating the samples of $37 < Y < 62$ above 648°C, one directly crosses the liquidus. In the range $25 < Y \leq 100$ and $610 < T < 648$, there are two areas of coexistence of α-MnNa + liquid with a shallow minimum of solidus/liquidus at (75, 610).

The previously determined (6) phase diagram of the MnV_2O_6–$LiVMoO_6$ system is recalled in Fig. 4b. The diagrams are similar. Minor differences consist in (i) a lower peritectic temperature and longer peritectic line for L = Na (62, 648) as compared to L = Li (48, 710), and (ii) a minimum of solidus line for MnNa (75, 610) which does not exist for MnLi; this is due to smaller ΔT between the peritectic temperature and melting point of $NaVMoO_6$ as compared to the analogous ΔT in the Li-containing system.

4. CONCLUSIONS

MnV_2O_6 (below 540°C) and $NaVMoO_6$ are known to crystallize in the brannerite-type structure, referred to as

TABLE 3
Octahedral Ionic Radii r_6 (Å) of the Considered Ions and the Relative Changes $\Delta r\%$ between the End Members of MnNa and MnLi Series of Solid Solutions

V^{5+}	Mo^{6+}	1/2 $\Delta r\%$ (Mo/V)	Mn^{2+}	Na^{1+}	$\Delta r\%$ (Na/Mn)	Li^{1+}	$\Delta r\%$ (Li/Mn)	Ref.
0.465	0.498	*3.5*	0.823	1.092	*32.7*	0.728	*−11.5*	(11)
0.54	0.59	*4.6*	0.83	1.02	*22.9*	0.76	*−8.4*	(12)

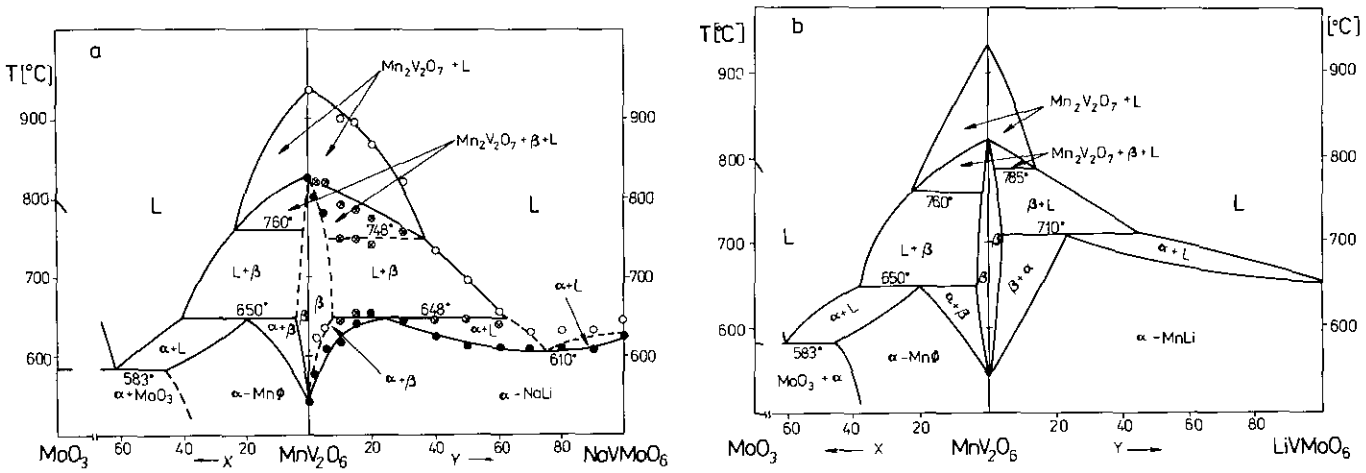

FIG. 4. (a) Phase diagram of the pseudobinary MnV_2O_6–$NaVMoO_6$ system based on DTA and X-ray investigations. Solid circles, onset temperatures of endothermal effects; open circles, endings of endothermal effects; crosses, estimated positions of shoulders or poorly separated peaks, tentatively estimated boundaries are drawn with dashed lines. On the left the coincidence is shown with the previously determined (8) diagram of the MoO_3–MnV_2O_6 system. α and β denote a low temperature (brannerite) and high temperature polymorphs of MnNa, respectively; L, liquid. (b) The previously determined (6) phase diagram of the MnV_2O_6–$LiVMoO_6$ system (after (8)).

α (1, 4, 8). Each of them can be doped with MoO_3 and solid solutions are formed, respectively, α-Mnϕ = $Mn_{1-x}\phi_xV_{2-2x}Mo_{2x}O_6$ with X_{max} = 45 (6) and α-Naϕ = $Na_{1-x}\phi_xV_{1-x}Mo_{1+x}O_6$ with X_{max} = 30 (3, 4) (ϕ, cation vacancy in the original Mn or Na site).

As shown in the present work, α-MnV_2O_6 and NaVMoO_6 reveal the miscibility in the entire composition range and form solid solutions α-MnNa = $Mn_{1-y}Na_yV_{2-y}Mo_yO_6$. α-MnNa solid solutions may be treated as matrices able to incorporate an excess of Mo^{6+} ions compensated by the equivalent number of cation vacancies in the Mn/Na sublattice. This results in formation of solid solutions α-MnNaϕ = $Mn_{1-x-y}\phi_xNa_yV_{2-2x-y}Mo_{2x+y}O_6$ belonging to the pseudoternary MnV_2O_6–$NaVMoO_6$–MoO_3 system. The stability range of α-MnNaϕ extends over about 60% of the area of the MnV_2O_6–$NaVMoO_6$–MoO_3 composition triangle and is bordered by a curve passing through the (X, Y) points (45, 0), (33, 30), and (30, 70). None of the studied α-MnNaϕ samples melted or decomposed below 530°C. As it results from the determined phase diagram of the pseudobinary MnV_2O_6–$NaVMoO_6$ system, the limit of thermal stability of α-MnNa extends between the (Y, T) points (0, 540), (25, 648), (75, 610), and (100, 623). The phase diagram shows (i) narrow double-lens-type solidus–liquidus gap at high values of Y, with a shallow minimum at Y = 75 and T = 610°C, (ii) two peritectic meltings at lower Y (yielding the high temperature β-MnNa polymorph at 648°C and $Mn_2V_2O_7$ at 748°C), and (iii) a small area of β-MnNa within $540 < T < 825$ with Y_{max} = 8 at 648°C.

The determined lattice parameters of the MnNa series of solid solutions reveal small deviations from Vegard's law. The unit cell increases along the series in all directions because the ionic radii of both dopants (Mo^{6+} for V^{5+} and Na^+ for Mn^{2+}) are larger than those of mother ions. However, the "growth" of the unit cell is anisotropic. Parameter c is strongly sensitive to Na/Mn substitution; b is ruled by Mo/V substitution; a is weakly influenced by Mo/V. This is a simple consequence of the sequence and tightness of packing of the distorted AO_6 and BO_6 octahedra in the brannerite-type structure.

Close analogy to the properties of the MnV_2O_6–NaVMoO_5–MoO_3 and MnV_2O_6–$LiVMoO_6$–MoO_3 (6) systems is observed. There are only two significant differences: (i) a monophasic area behind the boundary of saturated MnLiϕ and a multiphasic area outside the saturated Mn Naϕ, and (ii) an increase of the lattice parameter c along MnNa series and its decrease along MnLi, which is due to the fact that c is ruled by L/Mn substitution and the ionic radius of Li^+ is smaller than that of Mn^{2+}.

REFERENCES

1. K. Mocała and J. Ziółkowski, *J. Solid State Chem.* **69,** 299 (1987) and papers quoted therein.
2. R. Ruh and A. D. Wadsley, *Acta Crystallogr.* **21,** 974 (1966).
3. J. Gally, J. Darriet, and B. Darriet, *C.R. Acad. Sci. Paris, Ser. C* **264,** 1477 (1967).
4. B. Darriet and J. Galy, *Bull. Soc. Fr. Mineral. Cristallogr.* **91,** 325 (1868).
5. B. Masłowska and J. Ziółkowski, *J. Solid State Chem.* **87,** 208 (1990).
6. J. Ziołkowski, K. Krupa, and K. Mocała, *J. Solid State Chem.* **48,** 376 (1983).
7. P. Courty, H. Ajot, and C. Marcilly, *Powder Technol.* **7,** 21 (1973).
8. R. Kozłowski, J. Ziółkowski, K. Mocała, and J. Haber, *J. Solid State Chem.* **35,** 1 (1980).
9. JCPDS 1973, 9-387.
10. S. C. Abrahams and J. M. Reddy, *J. Chem. Phys.* **43,** 2533 (1965).
11. J. Ziołkowski, *J. Solid State Chem.* **57,** 269 (1985).
12. R. D. Shannon, *Acta Crystallogr. Sect. A* **32,** 751 (1976).